A novel process route for the production of spherical LBM polymer powders with small size and good flowability

Jochen Schmidt, Marius Sachs, Christina Blümel, Bettina Winzer, Franziska Toni, Karl-Ernst Wirth and Wolfgang Peukert*

Institute of Particle Technology, University of Erlangen-Nuremberg, Cauerstraße 4, D-91058 Erlangen, Germany

Authors email address:

jochen.schmidt@fau.de (J. Schmidt), marius.sachs@fau.de (M. Sachs),

christina.bluemel@fau.de (C. Blümel), bettina.winzer@fau.de (B. Winzer),

franziska.toni@fau.de (F. Toni), karl-ernst.wirth@fau.de (K.-E. Wirth),

wolfgang.peukert@fau.de (W. Peukert)

* Corresponding author:

Prof. Dr.-Ing. Wolfgang Peukert

Tel. +49 9131 8529400

Fax: +49 9131 8529402

Email: wolfgang.peukert@fau.de

Graphical Abstract
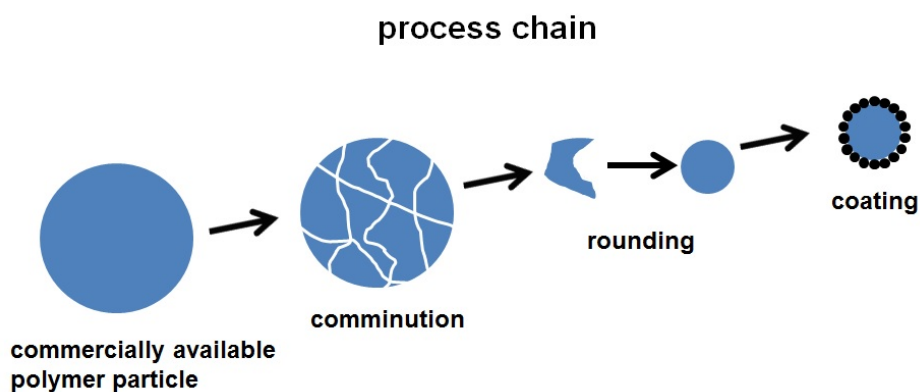
Highlights

- new process chain for producing LBM polymer powders with good flowability

- wet grinding of commercially available polymer granules allows for small product size

- rounding of polymer grinding product in a downer reactor

- nanoparticulate surface modification by dry coating increases surface roughness

- improvement of flowability of rounded polymer microparticles by dry coating

Keywords

polymers

wet grinding

downer reactor

dry particle coating

flowability

laser beam melting (LBM)

Abstract

Rapid prototyping has been applied so far in the production of special parts at low piece numbers. Currently, 'rapid prototyping' gradually is transferred to additive manufacturing opening new applications. At present basically only polyamide (PA) is available as an optimized powder material showing satisfying behavior during processing in Laser Beam Melting (LBM). Other types of polymer powders produced by cryogenic grinding show poor powder flowability as well as an unfavorable particle habitus resulting in poor device quality. In fact, it is challenging to produce laser sintering powders with small particle size, good flowability and processability.

We present a novel process chain for the production of spherical polymer micron-sized particles of good flowability that can be applied to a large variety of polymers: in a first step polymer particles are produced by a wet grinding method that are rounded in a second step using a heated downer reactor. To increase the flowability of the cohesive spherical polymer particles further nanoparticles are adhered to the particle surface in the third step. We demonstrate an increase of powder flowability by a factor of 5. The influence of particle habitus and nanoparticle functionalization on powder flowability is discussed in detail.

1. Introduction

Rapid prototyping applications are mainly applied in the production of special parts at low piece numbers offering the possibility to produce tailor-made designs by formless manufacturing. Currently, an increasing demand to widen the field of application is noticeable, i.e. 'rapid prototyping' gradually is transferred to additive manufacturing.

However, up to now there are still several major restrictions [1]: Besides limitations that are due to intrinsic peculiarities of beam-based additive manufacturing processes like laser beam melting (LBM), c.f. processing speed, one drawback is the very limited range of powder materials commercially available. In the case of LBM, for example, currently only polyamide (PA) is available as an optimized powder material with good flowability and optimized behavior [2, 3]. At present polyamide makes up 95% of the total market of laser sintering powders [1]. So far, other types of polymer powders have been evaluated for LBM processes e.g. produced by cryogenic grinding. These materials frequently show poor powder flowability and, thus, low packing density, unfavorable particle habitus and often inappropriate particle size distributions [4]. In fact, it is a highly challenging task to produce laser sintering powders with good flowability and processability: with decreasing particle size the ratio of van der Waals force and weight increases leading to agglomeration [5]. In consequence, powder deposition problems during LBM processes need to be overcome. Additionally, poor powder flowability frequently is accompanied by low bulk density [6]. In consequence, pores and inhomogeneities in the packed bed occurring during powder deposition of cohesive powders leads to poor quality of the resulting LBM processed devices.

We present exemplarily for polystyrene (PS) a process chain that is feasible for a large variety of polymer materials (see Figure 1): in the first step polymer micron-sized particles are produced by a wet grinding method proposed recently [7]. In a second step using a heated downer reactor, the irregular shaped particles obtained by comminution are rounded. To even further increase the flowability of the spherical micron-sized particles, nanoparticles are adhered to their surface by a dry particle coating process [8, 9].
The successful increase of powder flowability after the consecutive process steps has been monitored using a tensile strength tester [10, 11]. The influence of particle habitus and nanoparticle functionalization density on powder flowability is discussed.

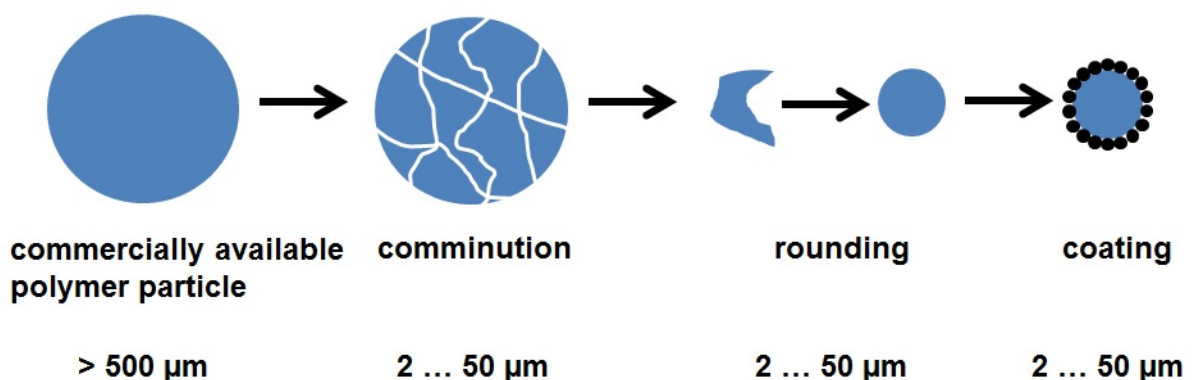| commercially available polymer particle	comminution	rounding	coating
> 500 µm	2 … 50 µm	2 … 50 µm	2 … 50 µm

Figure 1: Process chain for the production of spherically-shaped thermoplastic micron-sized particles.

2. Materials and methods

2.1 Materials

The approach proposed for the production of spherically-shaped polymer particles in the size range of 5 to 50 μm with good powder flowability has been exemplified for polystyrene (PS). As raw material amorphous PS (PS, Roth, granules sized approx. 4 mm) of a density of 1.05 g/cm^3 has been used. To obtain an appropriate feed particle size for the wet grinding process, the polymer granules have been pre-ground using a rotary impact mill Pulverisette-14 (Fritsch) equipped with a pin rotor and a 0.5 mm sieve ring at 20,000 min^{-1} using liquid nitrogen cooling. The particle size distribution of the PS feed material ($x_{50,3}$ = 123 μm) used for wet grinding is given in Figure 2. It exhibits a quite broad distribution with a $x_{10,3}$ of 40 μm and a $x_{90,3}$ of 263 μm (span ($x_{90,3}$-$x_{10,3}$) / $x_{50,3}$ = 1.80). For the wet grinding process denatured ethanol (95 %, VWR) has been used as solvent.

Fumed silica R1 (Evonik Industries) with a primary particle size of 7 nm has been applied for nanoparticulate coating of the broken and rounded micron-sized PS particles.
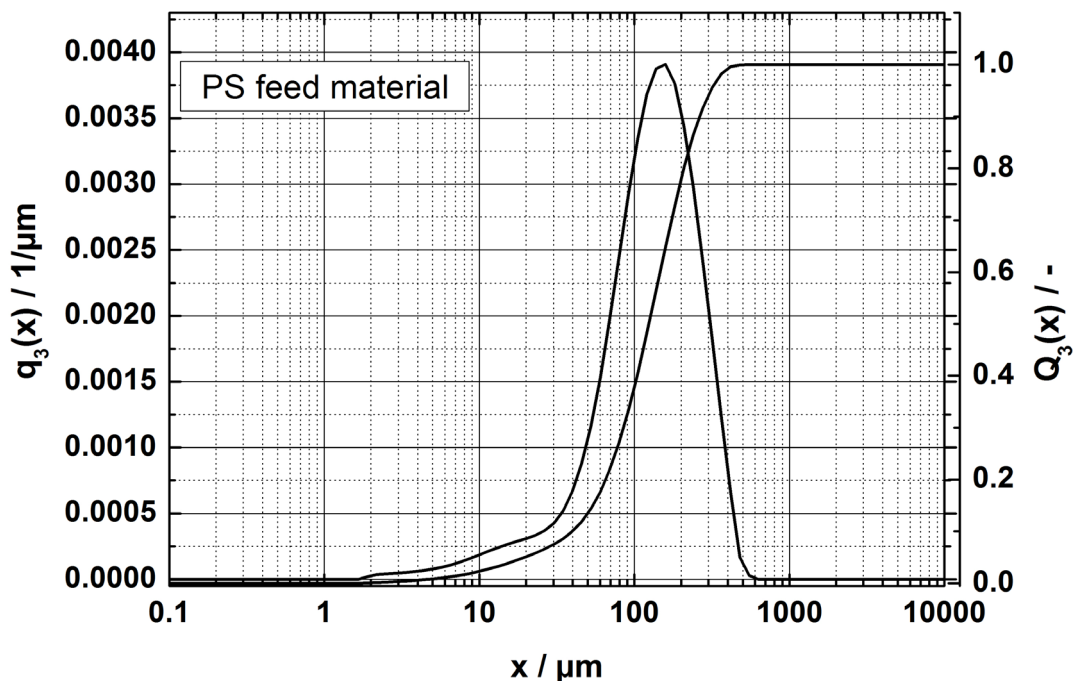

Figure 2: Particle size distribution (volume, density q_3 and cumulative Q_3) of the pre-comminuted PS feed material (Carl Roth) as determined by laser diffraction particle sizing.

2.2 Characterization methods

2.2.1 Differential Scanning Calorimetry (DSC)

DSC characterization of the PS particles was performed at a heating rate of 20°C min^{-1} using a DSC8000 (Perkin Elmer). The glass transition temperature of the PS feed material was determined to be T_g = 89.5 °C (see Supplementary Figure A). No pronounced change of the

glass transition temperature due to processing is observed: for the PS comminution product T_g = 90.2 °C was found. The rounded product exhibited a glass transition temperature of T_g = 90.9°C.

2.2.2 Laser diffraction particle sizing

Particle size distributions of the respective product suspensions obtained by the wet grinding process as well as of suspensions of the rounded particles have been determined by laser diffraction particle sizing using a Mastersizer 2000 / Hydro 2000S (Malvern). In the case of wet grinding, the concentrated ethanolic suspensions have been diluted as appropriate prior to measurement with deionized water under addition of small amounts of sodium dodecyl sulphate (SDS, 98% (Merck)) to ensure dispersion stability. In the case of rounded product particles appropriate amounts of the powder have been added to an aqueous SDS solution. Subsequent ultrasonic treatment has been performed to obtain a suitable dispersion for particle size measurements.

2.2.3 Scanning Electron Microscope (SEM)

The rounded polymer micron-sized particles as well as the quality of the nanoparticle coating have been characterized by scanning electron microscopy (SEM) using a Gemini Ultra 55 (Zeiss) device equipped with an InLens detector. An acceleration voltage of 1 kV has been used. SEM images were taken at appropriate magnifications in order to evaluate the coating quality of the composite particles obtained.

2.2.4 Powder flowability

Flowability measurements were conducted using a Zimmermann tensile strength tester [10] modified according to Meyer et al. [11]. The tensile strength tester is capable of determining inter-particle forces appearing in almost uncompacted powders. For details see section 2.4.4.

2.3 Experimental setup
2.3.1 Comminution (wet grinding)

Wet grinding experiments have been performed using a batch stirred media mill PE5 (Netzsch). Mass fractions of approximately 10 % and 19 % of milling material have been used in this study. A stress intensity (see section 2.4.1.) of $1.91*10^{-3}$ J was applied by setting the stirrer tip speed to 6.3 m s^{-1} equaling 800 min^{-1} and using Yttria-stabilized ZrO_2 grinding beads (YSZ, Tosoh) of a density of 6050 kg m^{-3} and a diameter of 2.0 mm. Approximately 14.3 kg of grinding beads have been introduced into the grinding chamber. The process temperature has been adjusted to 20 °C using the thermostat device unistat905w (Huber) and was kept constant to +/- 2 °C over the process time.

2.3.2 Rounding (downer reactor)

The particle rounding was performed in a downer reactor made of stainless steel with a length of 1,600 mm and a diameter of 25 mm equipped with a three stage heating system. Nitrogen (purity 5.0; Linde Gas) is used as carrier and sheath gas to minimize aging effects (oxidative degradation) of the treated polymer material. The edged polymer particles (PS) were dispersed using a PALAS RGB 1000 powder disperser with brush. The shear forces applied are known to be sufficient for deagglomeration of fine powders with a low density such as the polymer material used [12].

The aerosol was fed into the downer reactor where the polymer particles were molten and the rounding process was performed. The setup of the reactor and its aerosol inlet is outlined in Figure 3: In order to minimize the contact of molten polymer particles with the reactor walls, a special aerosol inlet is necessary. The polymer particle aerosol enters the downer reactor system in the center of the reactor cross section as a primary gas flow by an inner tube with a diameter of 10 mm. A secondary gas flow was applied as a sheath gas flow in order to guard the aerosol in the center of the cross section. The secondary gas flow enters the reactor zone using an outer tube with a diameter equal to the diameter of the downer reactor. To achieve a homogenous gas distribution, the secondary gas flow inlet is equipped with a sintered metal plate (GKN Sintermetals).
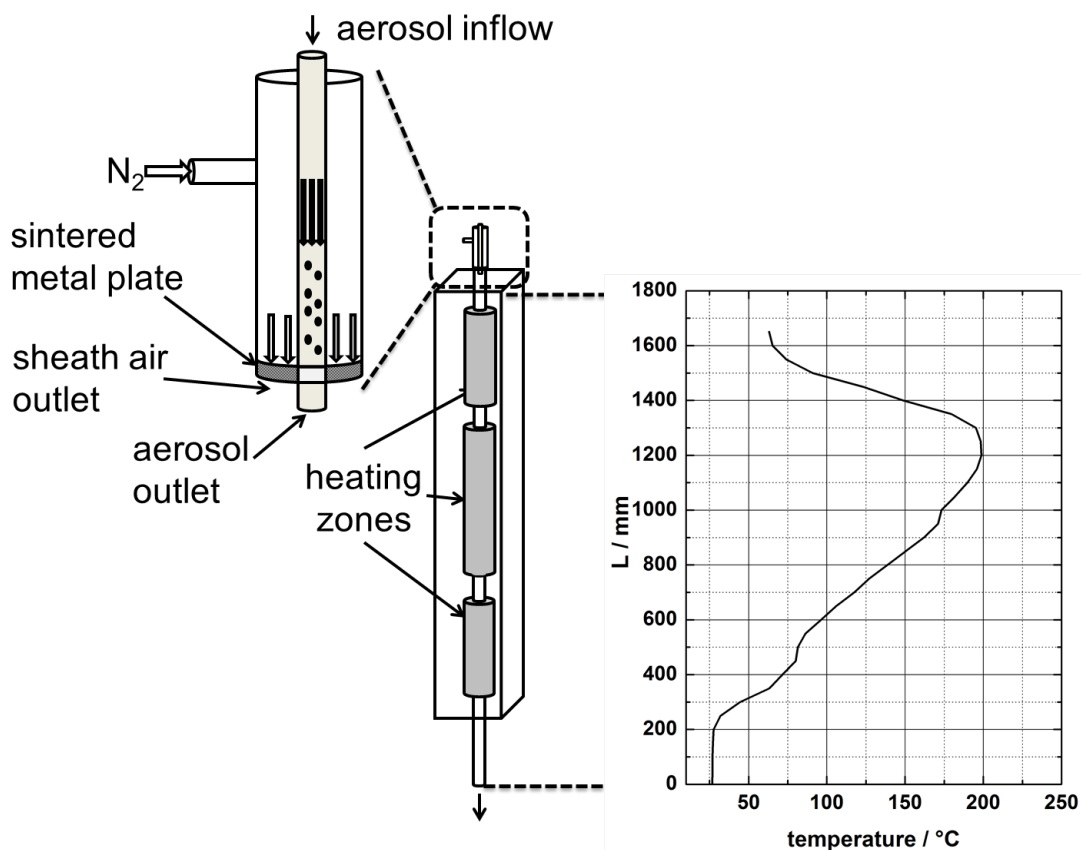
Figure 3: left: Downer reactor with aerosol inlet shown in detail, right: Temperature profile in the reactor system.

In order to determine appropriate temperature regimes for rounding of the PS comminution product in the downer reactor, the temperature profile for the different heating zones of the three stage heating system was determined using a Type K thermocouple.

Figure 3 shows the measured temperature distribution along the reactor length L (vertical direction). To melt the polymer, the temperature in the first heating zone of the downer reactor used is set 100 to 110 °C above the glass transition temperature of PS: The temperature in the consecutive two heating zones is subsequently lowered to achieve a stepwise solidification of the spherical particles. Moreover, this stepwise reduction of temperature allows to minimize any degradation of the polymer during the rounding process. Heating well above the glass transition temperature of the polymer is still necessary in the second heating zone allowing for complete rounding of the irregular particles (for details see section 2.4.2.). The last cooling step to room temperature was achieved by a reactor part without a heated surrounding. At the reactor outlet the rounded polymer product particles were collected onto a PTFE filter membrane (BOLA) with a pore diameter of 0.2 μm.

2.3.3 Dry particle coating

Dry particle coating processes of comminuted (irregular) and rounded PS host particles, respectively, were conducted using a tumbling mixer (T2F, Willy A. Bachofen AG). The PS host particles were mixed at 49 min^{-1} in an aluminum bottle of a total volume of 300 ml for 1 hour applying 1.0 wt% hydrophobic fumed silica guest particles R1 to obtain a homogeneous distribution of guest particles on the host particle surface.

2.4 Theoretical background

2.4.1 Wet grinding in stirred media mills – stress energy and stress number

Grinding in stirred media mills can be described according to Kwade [13] by the quantities stress energy SE and stress number SN where the mass specific energy is given by the product of SE and SN. SE_{max}, the maximum energy that may be transferred to a product particle upon collision of two grinding media (see equation 1), equals the kinetic energy of the grinding media scaled with a factor Φ taking the respective Young's moduli of grinding media and feed material into account [14-16]:

(eq. 1) $$SE_{max} \propto d_{GM}^3 \cdot v_{tip}^2 \cdot \rho_{GM} \cdot \Phi = d_{GM}^3 \cdot v_{tip}^2 \cdot \rho_{GM} \cdot \frac{E_{GM}}{E_{mat} + E_{GM}}$$

d_{GM}: grinding bead diameter, v_{tip}: stirrer tip speed, ρ_{GM}: density of grinding beads, E_{GM}: Young's modulus of the grinding media, E_{mat}: Young's modulus of the feed material.

In the case of polymer feed material and zirconia grinding beads this energy transfer coefficient Φ is close to unity [7]. Due to dissipation phenomena like e.g. viscous dampening (see [7, 16, 17] for details), the stress energy actually transferred to the product particles SE_{mat} (see equation 2) may be substantially lower than SE_{max}.

$$\text{(eq. 2) } SE_{mat} \propto SE_{max} \cdot \Phi \cdot r_\eta = d_{GM}^3 \cdot v_{tip}^2 \cdot \rho_{GM} \cdot \frac{E_{GM}}{E_{mat} + E_{GM}} \cdot \left(1 + \frac{1}{St_{GM}} \cdot \ln\left(\frac{x}{d_{GM}}\right)\right)^2$$

$$\text{with } St_{GM} = \frac{v_{GM} \cdot d_{GM} \cdot \rho_{GM}}{9 \cdot \eta}$$

St_{GM}: Stokes number of grinding media, x: product particle diameter, v_{GM}: velocity of grinding media, η: suspension viscosity. All stress energies SE_{mat} mentioned below have been calculated according to equation 2.

The definition of the stress number SN is given by equation 3. It depends on the concentration of the product suspension c_v, stirrer speed n, process time t, grinding bead diameter d_{GM}, the volume fraction of the grinding beads φ, and packing density $(1-\varepsilon)$.

$$\text{(eq. 3) } SN \propto \frac{\varphi \cdot (1 - \varepsilon)}{(1 - \varphi \cdot (1 - \varepsilon)) \cdot c_v} \cdot \frac{n \cdot t}{d_{GM}^2}$$

2.4.2 Downer reactor for particle rounding

The effect of surface tension on the shape of fluids and solids in a molten state is well-known [18, 19]: the fluid attempts to minimize the total surface area and, thus, will form a spherical shape. This effect is used to round the irregular particles obtained by the grinding process. The downer reactor offers the possibility to melt single particles whilst minimizing the contacts between two or more particles as well as the hot reactor walls.

By a concurrent flow of particles and gas back-mixing of the gas can be avoided [20] allowing a well-defined residence time distribution (RTD) of particles [21]. This aspect is important since polymer particles tend to age at elevated temperature [22], i.e. thermal degradation of the polymer chains and molecular structures may lead to reduced mechanical strength [23]. A narrow RTD of the particles in the heated reactor zones adjusted to the melting times minimizes simultaneously aging effects.

In order to estimate the time necessary to heat the feed to the gas temperature in the melting zone of the downer reactor the heat transfer rate from gas (in this case nitrogen) to the polymer core (here PS) is calculated. Due to the low temperatures any heat exchange due to radiation can be neglected. In our case, heating of the polymer particles to the melting temperature is mainly due to convective and, respectively, conductive heat transfer from the surrounding gas to the particles.

The change of the internal energy of the particles equals the heat flow from the gas to the particle. The heat transfer is calculated assuming Nu=2.

(eq. 4) $c_{p,P}\rho_P\frac{\pi}{6}x^3\Delta\dot{T} = -2\pi x\lambda_g\Delta T$

$c_{p,P}$ is the specific heat capacity of the polymer, λ_g the thermal conductivity of the surrounding gas, T the temperature, ρ_p: polymer particle density, x: polymer particle diameter.

The starting temperature difference ΔT_0 is given by the difference of the respective gas temperature which was determined to T_{Gas}= 473 K (see Figure 3) and the particle's temperature which was assumed to ambient temperature ($T_{Particle}$ = 293 K). The time t necessary for heating the feed to $0.99*T_{Gas}$ was estimated by equation 5 taking $\Delta T = 0.01*\Delta T_0$ into account.

The solution of equation 4 with respect to the temperature increase ΔT with time t and a constant temperature of the surrounding gas is as follows:

(eq. 5) $\frac{\Delta T}{\Delta T_0} = exp\left[-12\frac{\lambda_G t}{\rho_P c_{p,P} x^2}\right]$

The values for the heat properties of polymer and nitrogen were set to $c_{p,P}$ =1070 Jkg^{-1}K^{-1} for PS [24] and λ_G = 0.0361 Wm^{-1}K^{-1} for nitrogen [25].

The time for reaching only 1% of the original temperature difference between gas and particle is determined to 1.5 ms and 37 ms for a particle size of x = 10 µm and 50 µm, respectively, i.e. heating of the PS particles under consideration is achieved at time scales in the order of magnitude of several 10 ms. Enthalpies due to the phase transition and changes of heat capacity due to heating and phase transition can be neglected in the above estimations due to the amorphous state of the polymer: the change of $c_{p,P}$ due to the phase transition at the glass transition point was measured to be only 220 J*kg^{-1}*K^{-1}. The energy due to glass transition of a single polystyrene particle with a diameter of 12 µm is $2\cdot10^{-8}$ J (assumption: width of the glass transition temperature range is 10 K, c.f. Supplementary Figure A). The heat flow associated with glass transition is only 1.1 % of the internal energy consumed upon heating a single 12 µm PS particle from 25 °C to 200 °C.

The required residence time necessary for particle rounding depends on the melt viscosity of the polymer and the surface energy. Actually, the characteristic sintering times of non-spherical particles need to be considered (c.f. e.g. [26-30]). In a recently published paper by Kirchhof et al. [30] the viscous-flow aggregate sintering of three-dimensional particle aggregates has been simulated by solving the Navier-Stokes equations by the fractional volume of fluid method. They outlined the effect of the number of interparticle contacts within the aggregate and of the agglomerate structure on the sintering kinetics. These results can

be transferred to the rounding process in order to estimate characteristic times necessary to obtain a spherical shape from an irregular particle.

An irregular polymer particle obtained by the wet-grinding process shows a rather complex geometry. For our considerations we assumed that the ground particle can be seen as a structure comparable as seen in Figure 4. This structure consists of a sphere with humps in a size of approximately 1-2 µm. This approach allows us to derive an upper estimate of the necessary times for the sintering process and different arrangements of the single spheres. Thus, a wide range of possible particle morphologies obtained by the grinding process is covered by this approach.
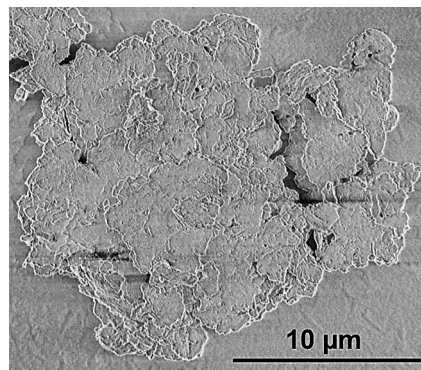

Figure 4: Irregular polymer particle after the grinding process.

The simulation by Kirchhof et al. [30] reveals that independent of the initial shape (e.g. linear chain or 3 D dumbbell) of the initial aggregate with a mean coordination number of $N_k = 1.8$ a dimensionless time to reach finally a spherical particle can be determined. A spherical particle of radius $x_f = \sqrt[3]{N} \cdot x_0$ consisting of N = 10 primary particles of diameter x_0 is obtained after a dimensionless sintering time of $t_{sintering}$ = 1.12 (see equation 6, for details see [30]). Particles with a denser structure and higher coordination number will sinter considerably faster.

(eq. 6) $t_{sintering} = \dfrac{t\sigma}{\eta x_f} = 1.12$

To convert the dimensionless sintering time $t_{sintering}$ to the sintering time t that applies to PS material parameters reported in literature have been used: The viscosity η for PS melt was set to $\eta = 7 \cdot 10^3$ Pa*s [28], the surface tension of the material at 200 °C is estimated to σ =30 mN*m^{-1} [29]. According to the measured particle size distribution (see Figure 9) x_f has a value of 5 µm. Using the method of Kirchhof et al. a sintering time of particles of radius x_f = 10 µm of t = 2.6 s (see equation 6) is estimated as an upper estimate. In a typical experiment an average residence time for a total volume flow of 1.04 m³h^{-1} of 2.7 s (assuming a laminar flow regime, Re = 418) at a maximum process temperature of 200 °C is

achieved. Possible thermal degradation of the polymer due to the rounding process is insignificant: In LBM processing of polymers process times of several hours are typical where the laser sintering powders are kept at temperatures slightly (approx. 20 K) below the melting temperature.

Table 1 summarizes physical properties for some polymers suitable for LBM. Moreover, sintering times necessary for rounding of 10 µm particles estimated according to the method proposed by Kirchhof et al. [30] and appropriate reactor lengths are specified. According to the viscous flow sintering model sintering times necessary for rounding (at constant primary particle number N) scale with diameter x, i.e. for aggregates sized several 10 microns quite long residence times are required for rounding of polymers. Besides particle size melt viscosity mainly determines the necessary residence times for rounding.

Table 1: Physical properties of different polymer materials [31-33] and estimated sintering times (for x_f = 10 µm) and reactor lengths necessary (for details see text).

Material	PS	PBT	POM
Interfacial Tension σ / Nm^{-1}	0.03	0.042	0.03
Viscosity η / Pas	7000	300	31000
Sintering Time / s (for x_f = 10 µm)	2.61	0.1	13
Reactor length / m (d = 25 mm, $\dot{V}$=1.04 m³*h⁻¹)	1.54	0. 05	6.81

The shown sintering times have been calculated for particles with a primary particle size **x_0** of 1 µm and N = 10 primary particles. Following Eq. 6 the value of a_0 influences the sintering times linearly. The calculated necessary reactor length following a total volume flow $\dot{V}$ of 1.04 m³*h⁻¹ and a diameter of the downer reactor d of 25 mm agrees well with the obtained results for PS and have to be verified for PBT and POM in future experiments.

2.4.3 Dry particle coating

Dry particle coating is a cost-efficient, scalable mixing process for assembling tailor-made composite particles [6, 8, 9] in order to increase powder flowability and bulk density of the packed bed. Nanoscale guest particles are attached to the surface of micron-sized host particles by van der Waals forces. The distance between the individual host particles is increased by the adhesion of nanoparticles which leads to a reduction of the overall adhesion forces [34, 35] between the functionalized host particles. This mechanism follows the well-known model according to Rumpf [36]. Van der Waals forces are reduced due to an increase of surface roughness of the particles: "Spacers" (guest particles) are attached to the host particle surface which enlarge the interparticle surface distance and, thus, influence the adhesion force as summarized in Figure 5 (left).

Depending on the size of the host particles, there is an optimum size of guest particles leading to a minimum van der Waals force. Figure 5 (right) depicts the dimensionless adhesion force (calculated by dividing the van der Waals force between two rough spheres by the van der Waals force between two smooth spheres) in dependence on guest particle radius r for different host particle radii R (5 µm and 30 µm) at constant interparticle distance a. In the case of micron-sized host particles typically guest particles sized smaller than 10 nm are most effective in terms of reduction of adhesion force.

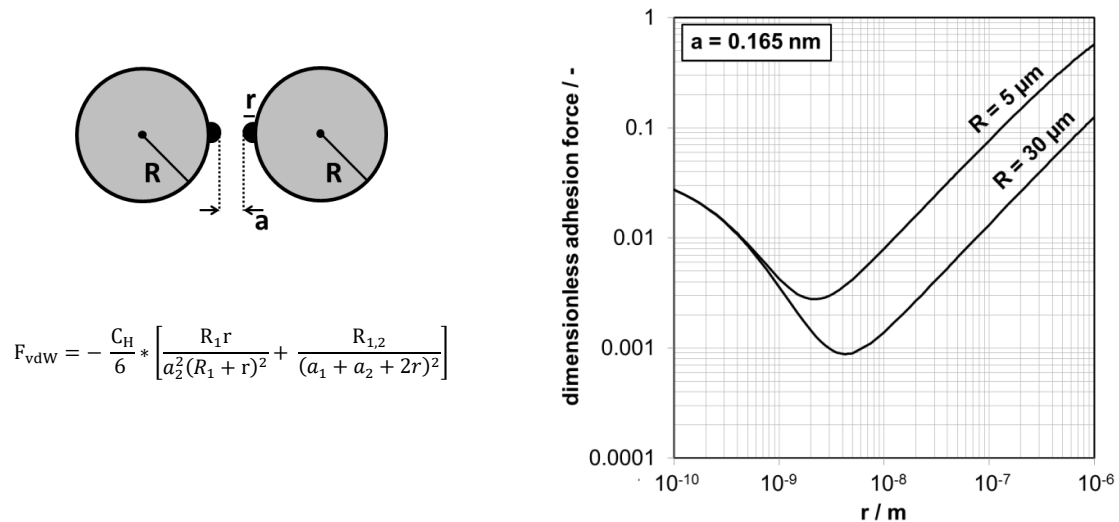$$F_{vdW} = -\frac{C_H}{6} * \left[\frac{R_1 r}{a_2^2 (R_1 + r)^2} + \frac{R_{1,2}}{(a_1 + a_2 + 2r)^2} \right]$$

Figure 5: Left: van der Waals force between two spheres (of radius R) with an asperity of curvature r according to Tomas [37]; right: relative van der Waals force between host particles of radius R of different particle surface roughness (r, parameter of surface roughness).

2.4.4 Tensile strength tester

Tensile strength allows for predictions of powder flowability. It is indirectly proportional to the flowability, i. e. with decreasing tensile strength flowability increases. Moreover, the tensile strength tester is an appropriate device to investigate adhesion forces in almost uncompacted bulk such as the powder bed in a LBM machine. Furthermore, only a small amount of powder (4.6 mm³) is necessary to obtain experimental data on flowability. The working principle of this device is outlined in Figure 5.

(a) Preparation of initial state: The flat surface of an aluminum plate (stamp) is coated with a thin layer of petroleum jelly prior to each investigation. The powdered samples were sieved into a flat aluminum container with a depth of 5 mm and a diameter of 34.3 mm. Afterwards the powder surface was smoothed by a doctor blade without compacting it.

(b) Starting the investigation, the aluminum container with the powder inside is moved towards the aluminum plate with a constant speed of 3.4 µms⁻¹ until the powder bed

within the aluminum container contacts the aluminum plate with a load of 153 Pa (= 0.6 g). This contact position is hold for 10 s.

(c) Afterwards the aluminum container is separated from the aluminum plate by moving it down with a speed of 1.7 µms^{-1}. The first layer of the powder in the aluminum container remains at the aluminum plate due to its attachment to the thin layer of petroleum jelly.
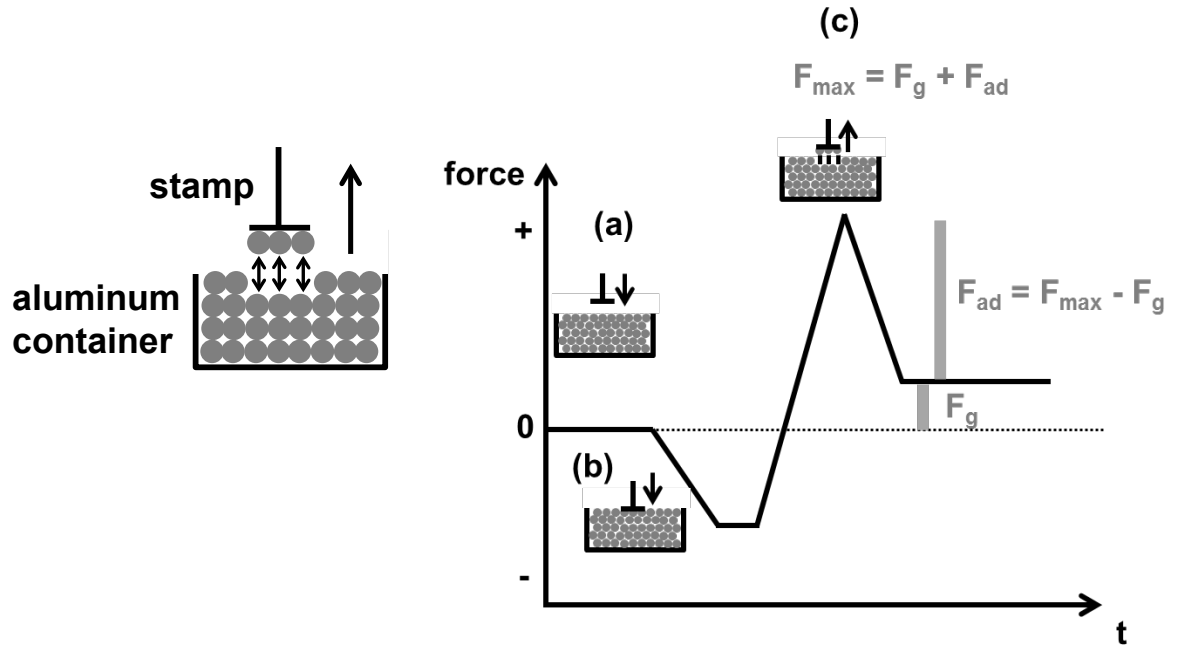

Figure 6: Sequence of a tensile strength measurement.

A load cell records concurrently the weight force. By separating the fixed powder layer from the loose powder packed bed F_{max} is measured. After separation of the powder layers only the weight force F_g of the particles attached to the stamp is recorded. By subtracting the maximum force F_{max} from the weight force F_g the adhesion force can be obtained. Dividing the adhesion force by the area of the stamp A_{stamp}, the tensile strength σ can be calculated according to equation 7.

$$\text{(eq. 7) } \sigma = \frac{F_{max} - F_g}{A_{stamp}}$$

3. Results

3.1 Wet grinding of polystyrene

The PS feed material ($x_{50,3}$ = 123 µm) has been subjected to wet grinding in denatured ethanol using the stirred media mill PE5 at 20 °C applying a stress energy of 1.91 mJ, i.e. a stirrer tip speed of 6.3 m s^{-1} and zirconia grinding media of 2.0 mm in diameter. Figure 6 summarizes the evolution of the particle sizes $x_{10,3}$, $x_{50,3}$, $x_{90,3}$ over process time for the

respective product at a feed concentration of 10.5 wt% and 18.9 wt% obtained under the aforementioned conditions. Whereas during the first hour of process time the grinding kinetics are faster for the grinding process at lower feed particle concentration as compared to the experiment at higher feed mass concentration (c.f. smaller $x_{50,3}$ and $x_{90,3}$ at comparable grinding times) after approximately 3 hours a product sized $x_{50,3}$ = 12.0 µm of similar particle size distribution (see Supplementary Figure B) is obtained for both feed concentrations Figure 7). The glass transition temperature of the comminution product as determined by DSC (T_g = 90.2 °C) as well as the change in specific heat (Δc_p = 0.25 J/g*K) at glass transition are comparable to the PS feed material (see Supplementary Figure A), i.e. (severe) degradation of the polymer during comminution is ruled out under the aforementioned conditions. The grinding kinetics of PS observed under the aforementioned conditions are similar to recent results [7] obtained under comparable stressing conditions and process temperature. As expected, with increasing process time the particle size distribution becomes narrower.

Prior to rounding, the PS product particles obtained after approximately 3 hours of grinding ($x_{50,3}$ = 12.0 µm) have been withdrawn from the ethanolic suspension by centrifugation and afterwards vacuum-dried at 60 °C.
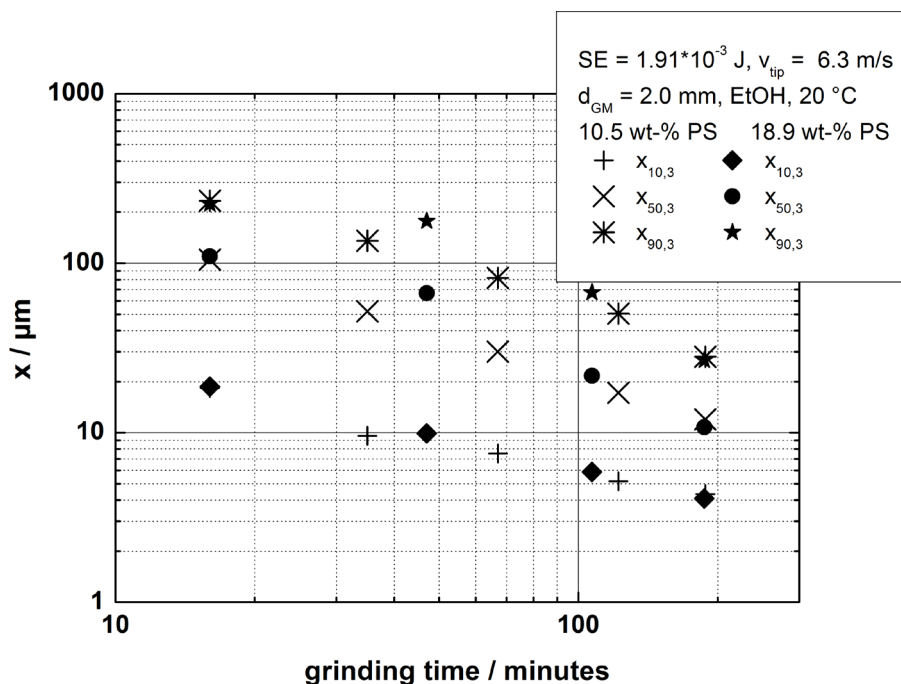

Figure 7: Particle sizes $x_{10,3}$, $x_{50,3}$ and $x_{90,3}$ of polystyrene (PS) in dependence on grinding time at constant stress energy SE: open symbols: 10.5 wt-% PS, filled symbols: 18.9 wt-% PS, 20 °C, SE = 1.91 mJ, 2.0 mm YSZ grinding beads).

3.2 Rounding of the ground PS particles

SEM imaging reveals that the rounding process leads to spherical polymer particles with a defined particle size distribution being, of course, similar to the PSD after the grinding process as sintering conserves the particle volume. SEM images of the rounded PS product obtained for a temperature setting of the three stage heating system of 200 °C / 150 °C / 100 °C, 0.8 m³h⁻¹ primary gas flow and 0.24 m³h⁻¹ secondary gas flow applying the comminution product ($x_{50,3}$ = 12.0 µm) as feed material are depicted in Figure 8. Under the aforementioned conditions an average residence time of 2.7 s applies and complete melting and resolidification of the PS particles is achieved. The particles obtained are almost perfectly spherical.
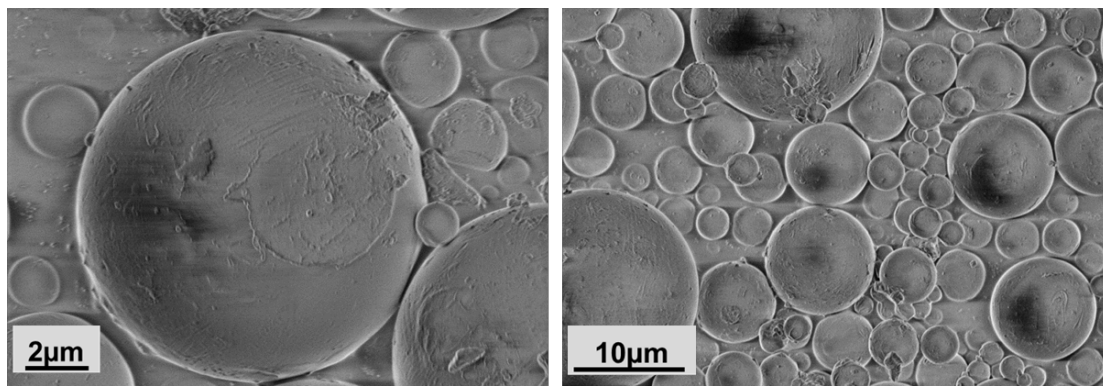

Figure 8: Spherical PS particles as obtained after the rounding process.

Cumulative particle size distributions Q_3 of the rounded product and the feed (comminuted PS) are shown in Figure 9. If only a change of particle habitus would take place the particle size distributions of irregular feed particles and rounded product would be identical. In the case of improper generation of the aerosol, such as bad dispersing, agglomerates would enter the downer reactor and melted particles that make up the agglomerate would coalesce and form a single spherical polymer product particle with a total particle volume being equal to the sum of the individual volume contributions of the particles the agglomerate consisted of. Also collisions of melted polymer particles and subsequent coalescence during rounding could lead to a shift in the particle size distribution to larger sizes. So far, in practice only a small shift of the volume averaged mean diameter $x_{50,3}$ of the rounded product as compared to $x_{50,3}$ of the comminution product to a larger particle size in the Q_3 distributions occcurs, i.e. the dispersing of the particles is efficient (agglomerates are destroyed) and any pronounced coalescence of the molten polymer droplets during rounding in the downer reactor has been avoided. The solid concentration (vol./vol.) in the nitrogen flow was $1 \times 10^{-6} \ \frac{m_{PS}^3}{m_{N_2}^3}$. Assuming that a volume element of the reactor is defined by a cubic array of single particles of same size, the distance between two particle surfaces can be calculated taking the aforementioned

geometrical arrangement and the particle diameter into consideration. In this case, for particles sized $x_{50,3}$ =12 µm an interparticle distance of 300 times the particle size or a total interparticle distance of 3 mm is obtained. The distance between single particles is necessary to avoid contact between particles in the molten state. An estimated maximum capacity of the downer reactor is around 10 times higher than the concentration applied in the experiments presented.

The maximum solid concentration in the gas flow of the downer reactor before direct contact between two single particles may occur is at least 10 times higher than the concentration applied in the experiments. Thus, considerable process intensification can be achieved by increasing the mass flow of polymer particles.
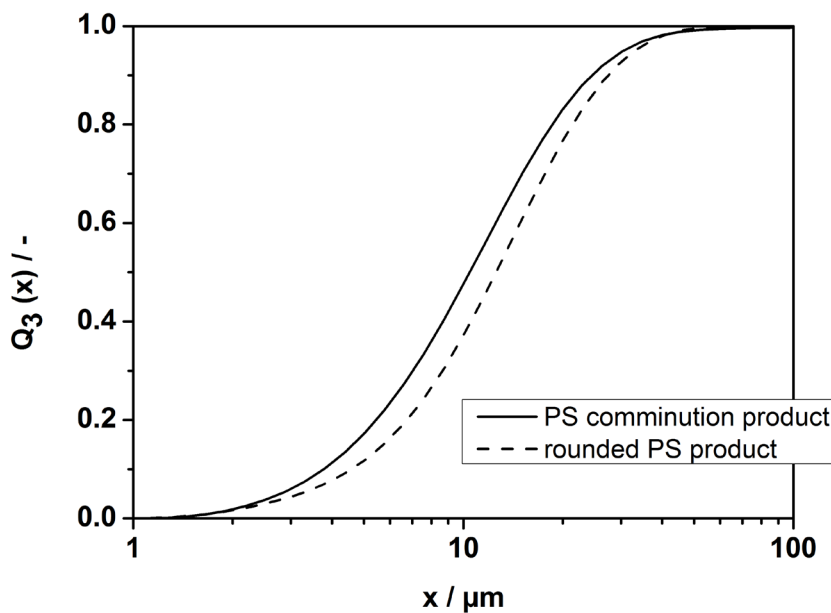

Figure 9: Cumulative particle size distributions Q_3 of the feed material (comminuted PS) and the product particles obtained after rounding process.

The results of the rounding process can the measured by determining the form factor of the different PS particles after the comminution and after the rounding process.

The sphericity of a particle is defined as the surface of a sphere with an equal volume divided by the surface of the measured particle. The maximum value of the sphericity Ψ, reached by a perfect sphere, is 1.

(eq. 8) $\Psi = \dfrac{d_V^2 \pi}{s}$

With d_V as the diameter of the volume equivalent sphere and S the measured surface of the investigated particle. The sphericity Ψ has been obtained by processing SEM images using the commercial image analysis software by AxioVision (Zeiss). The surface S of the particle can be estimated by the aforementioned software using an evaluation of the circumference of the particle after Crofton, which is a mathematical approach for the determination of the circumference of rather spherical objects. The density distribution of the form factors of both, the comminuted and the rounded PS particles are shown in Figure 10. A residence time of 2.7 s was applied. The rounding process leads to an increase of the sphericity from 0.3 - 0.6 for the particles after the wet grinding process to 0.9 - 1 for the rounded PS. This clearly shows that the treatment in the downer reactor proposed leads to a change in shape of the polymer particles.
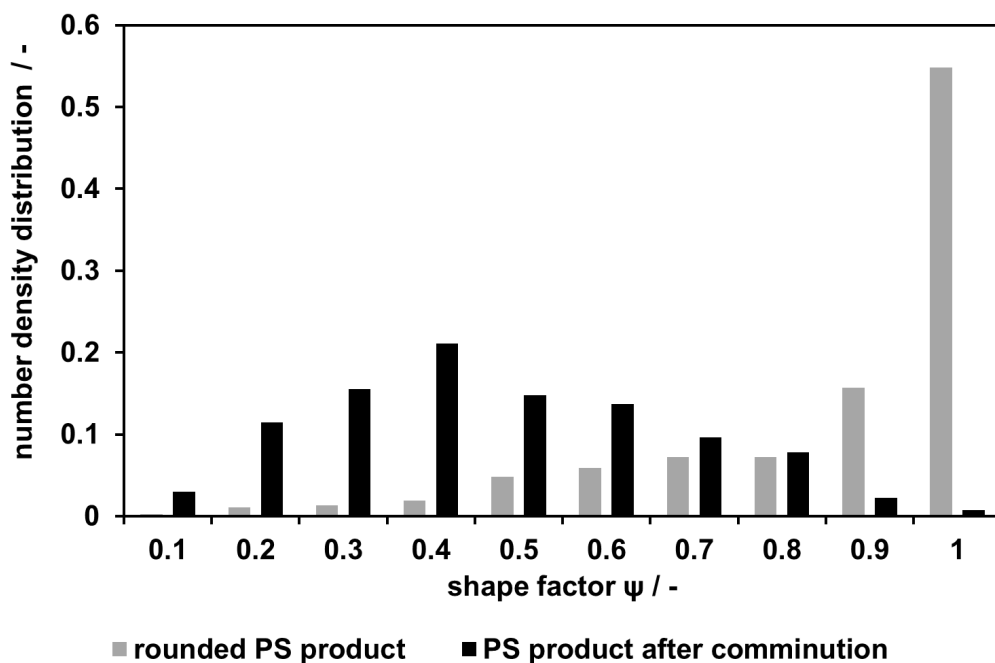

Figure 10: Form factor of the comminuted (grey) and the rounded PS product (black, 2.7 s residence time)

3.3 Dry particle coating and its influence on powder flowability

Figure 11 shows a rounded PS particle after the dry particle coating process applying 1 wt% fumed silica R1. The surface of the uncoated and rounded PS particles is mostly smooth (see Figure 8). SEM images of the composite particles at different magnifications clarify a consistently homogeneous coating with silica guest particles on the surface of the entire PS host particle (Figure 11) and thus an increase of surface roughness which improves powder flowability and reduce tensile strength, respectively.
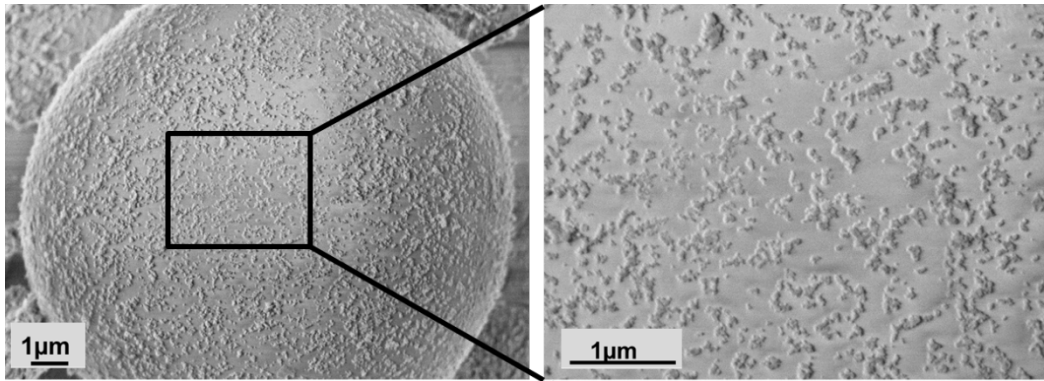
Figure 11: Homogeneous coating of PS host particle with fumed silica guest particle via dry particle coating process.

Data on tensile strength of powders obtained after the consecutive process steps, i.e. particles of different shape and surface roughness but comparable particle size distribution, are summarized in Figure 12: PS particles obtained after wet grinding show a high tensile strength of about 25 Pa and therefore a poor flowability. In comparison to the edged PS particles obtained by comminution, the rounded PS particles show a reduced tensile strength of only about 12 Pa and therefore are much less cohesive by more than a factor of 2. After the dry particle coating process the tensile strength of both powders, i.e. the edged and rounded PS particles, respectively, decreases. It is noticeable that the excellent flowability of the rounded and dry coated particles with a tensile strength of approximately 4 Pa is superior as compared to the edged and dry coated particles (tensile strength approximately 10 Pa). This demonstrates that besides roughness the particle shape has a significant influence on the powder flowability.
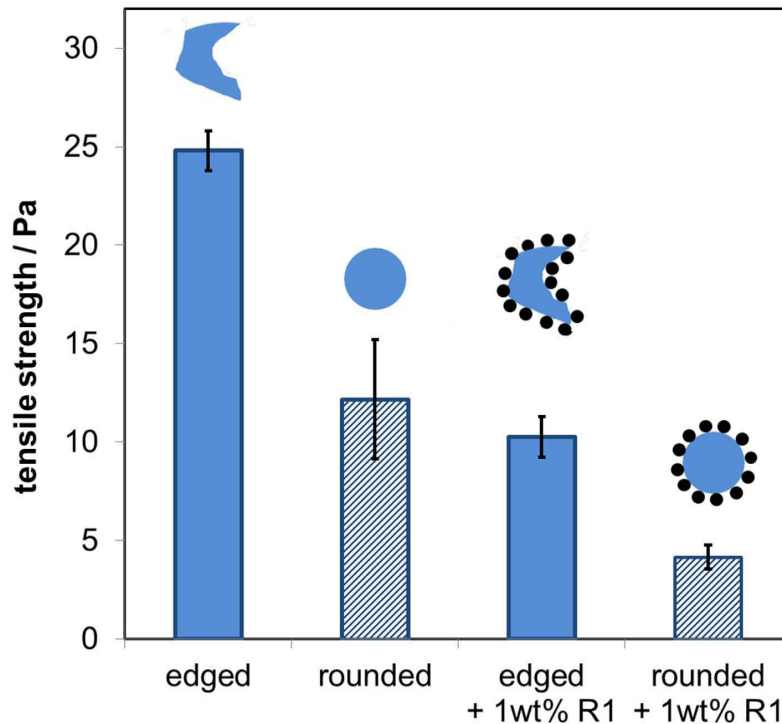
Figure 12: Results of tensile strength measurements: the tensile strength of the PS particles decreases (flowability increases) with rounding and dry particle coating with silica R1.

Conclusions

A process chain for the production of micron-sized polymer particles with good flowability comprising of wet grinding, a rounding process in a downer reactor and a dry coating step has been successfully established and exemplified for polystyrene (PS). Moreover, the improvement of powder flowability after the consecutive process steps, i.e. rounding of the comminution product and subsequent nanoparticulate coating (increase of surface roughness) has been monitored using a tensile strength tester: the rounded and dry-coated PS powder exhibits a reduced tensile strength of only about 20 % of the tensile strength of the edged PS comminution product, i.e. a remarkable improvement of powder flowability can be realized by rounding and dry coating. These properties allow the polymer powders to be applied in LBM processing.

Aging of the polymer powders due to thermal treatment during the rounding process is insignificant due to the short average residence times necessary which are only on the second time scale as estimated from literature data. It has been demonstrated that simulation results on viscous-flow sintering [30] taking particle size and material parameters (interfacial tension, melt viscosity) of the respective polymer into consideration allow for reliable reactor design. The approach proposed is not restricted to PS, i.e. it can be easily applied to a wide variety of other polymers relevant for LBM including e.g. PBT or POM which will be reported in a forthcoming paper. Moreover, all the individual process steps are

scalable: Scale-up of wet grinding processes in stirred media mills is well-established by considering the mass-specific energy introduced into the mill (see e.g. [38, 39]). Also the scalability of downer systems is well-known in literature. The mechanism of flow structures and heat mechanism in downer reactors with different reactor diameters as well as at different solid concentrations have been described in detail [20, 21]. The dry particle coating process is mainly affected by energy input. Investigations by Pfeffer et al. [40] have shown that the mechanism of dry particle coating is independent of the mixing device used. Due to scalability, the process chain can be transferred to the plant scale which in principle allows for commercial scale production.

Acknowledgements

Symbols

a	distance between particles (a_0 = 0.156 nm [41])	/ m
a_f	radius of the fully coalesced sphere	/ m
A_H	Hamaker constant	/ J
A_{stamp}	area of the stamp	/ m^2
$c_{p,P}$	specific heat capacity of the particle	/ J/(kgK)
C_V	concentration of the product suspension	/ kg/m³
d_{GM}	grinding media diameter	/ m
d_V	diameter of the volume equal sphere	/ m
E_{GM}	Young's modulus of the grinding media	/ Pa
E_{mat}	Young's modulus of the feed material	/ Pa
F_g	weight force	/ N
F_{max}	maximum force	/ N
F_{vdW}	van der Waals force	/ N
m_P	particle mass	/ kg
n	stirrer speed (number of revolutions)	/ 1/s
Nu	Nusselt Number $= \dfrac{Convective\ heat\ transfer}{Conductive\ heat\ transfer}$	/ -
r	radius of the guest particle	/ m
R	radius of the host particle	/ m
S	surface area	/ m^2

SE	stress energy	/ J
SN	stress number	/ -
St_{GM}	Stokes number of grinding media	/ -
T	Temperature	/ °C
T_{Gas}	gas temperature	/ K
$T_{Particle}$	particle temperature	/ K
t	process time	/ s
$\dot{V}$	volume flow	m^3/h
v_{tip}	stirrer tip speed	/ m/s
v_{GM}	velocity of grinding media	/ m/s
x	particle size	/ m

Greek letters

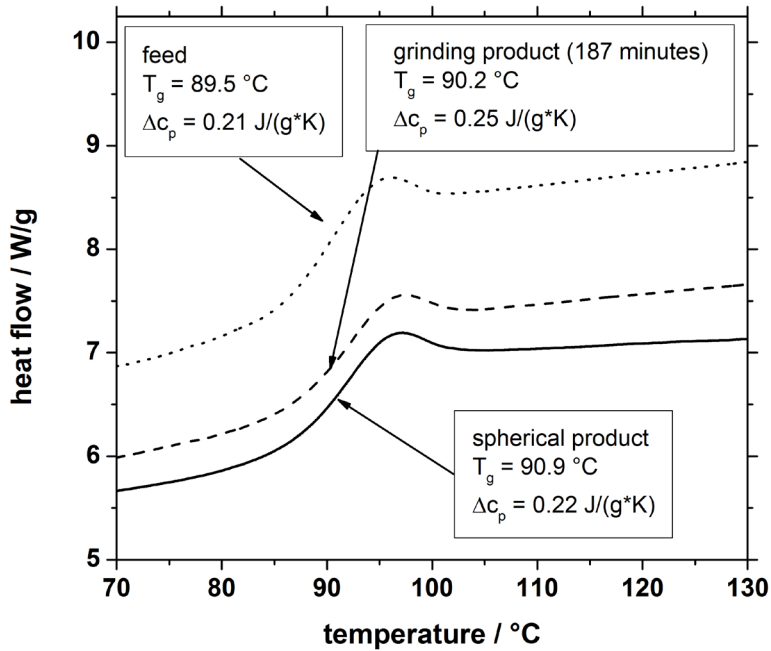| $(1- \varepsilon)$	packing density	/ -
φ	volume fraction of the grinding beads	/ -
η	viscosity	/ Pas
ρ_{GM}	density of grinding media	/ kg/m^3
ρ_P	particle density	/ kg/m^3
σ	tensile strength	/ Pa
σ	surface tension	/ mN/m
λ_G	thermal conductivity	/ W/mK
Ψ	sphericity	/ -

Supplementary Information

Figure A: Glass transition temperature of PS feed material (dotted line) ground material (dashed line) and rounded as determined by DSC (heating rate 20 °C / min).
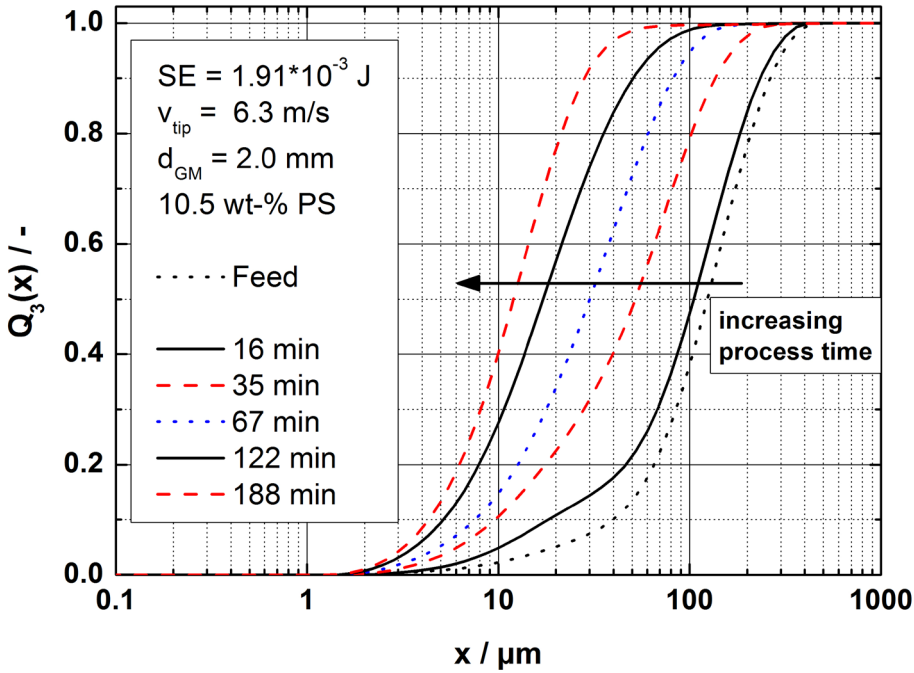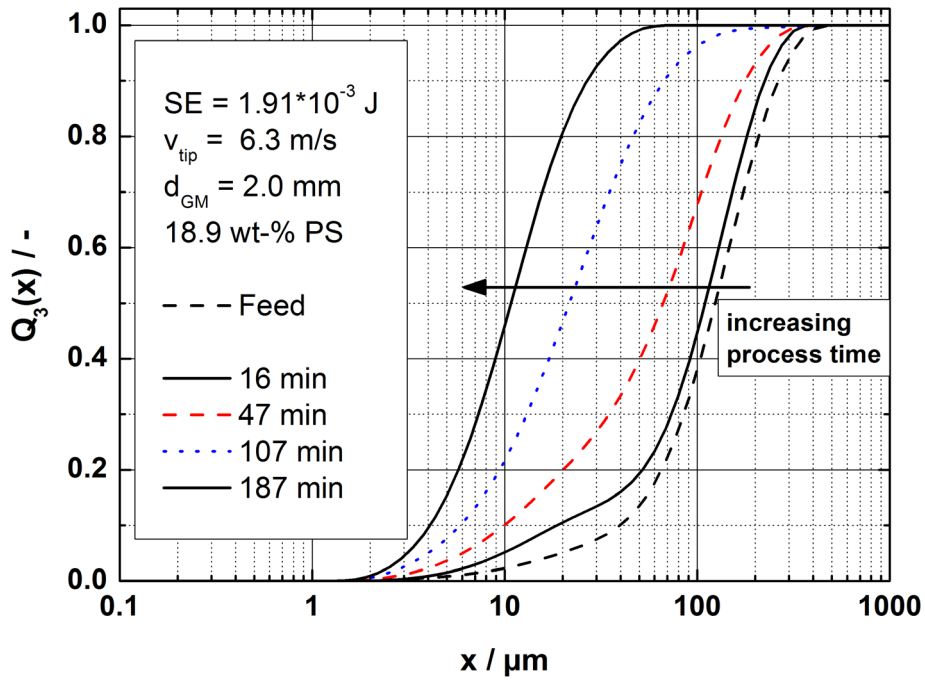
Figure B: Cumulative particle size distribution Q_3 of polystyrene (PS) in dependence on grinding time at constant stress energy SE: (a) 10.5 wt-% PS (20 °C, SE = 1.91 mJ, 2.0 mm YSZ grinding beads); (b) 18.9 wt-% PS (20 °C, SE = 1.91 mJ, 2.0 mm YSZ grinding beads).

Literature

[1] R. D. Goodridge, C. J. Tuck, R. J. M. Hague, Laser sintering of polyamides and other polymers, Progress in Materials Science 57 (2012) 229–267.

[2] B. Wendel, D. Rietzel, F. Kühnlein, R. Feulner, G Hüldner, E. Schmachtenberg, Additive Processing of Polymers. Macromol. Mater. Eng. 293 (2008) 799–809.

[3] D. Drummer, D. Rietzel, F. Kühnlein, Development of a characterization approach for the sintering behavior of new thermoplastics for selective laser sintering, Physics Procedia 5 (2010) 533–542.

[4] D. Rietzel, F. Kühnlein, D. Drummer, Selektives Lasersintern von teilkristallinen Thermoplasten. RTejournal - Forum für Rapid Technologie, 6 (2011) (urn:nbn:de:0009-2-31138)

[5] H. Schubert, Grundlagen des Agglomerierens, Chem. Ing. Tech., 51 (1979) 266-277.

[6] J. Yang, A. Sliva, A. Banerjee, R. N. Dave, R. Pfeffer, Dry particle coating for improving the flowability of cohesive powders. Powder Technol., 158 (2005) 21-33.

[7] J. Schmidt, J., M. Plata, S. Tröger, W. Peukert, Production of polymer particles below 5µm by wet grinding. Powder Technol. 228, (2012) 84–90.

[8] M. Linsenbühler, K.-E. Wirth, An innovative dry powder coating process in non-polar liquids producing tailor-made micro-particles. Powder Technol., 158 (2005) 3-20.

[9] S. F. Lux, T. Placke, C. Engelhardt, S. Nowak, P. Bieker, K.-E. Wirth, S. Passerini, M. Winter, H.-W. Meyer, Enhanced Electrochemical Performance of Graphite Anodes for Lithium-Ion Batteries by Dry Coating with Hydrophobic Fumed Silica. J. Electrochem. Soc. 159 (2012) A1849-A1855.

[10] A. Schweiger, I. Zimmermann, A new approach for the measurement of the tensile strength of powders Powder Technol. 101 (1999) 7 – 15.

[11] K. Meyer; I. Zimmermann; Effect of glidants in binary powder mixtures. Powder Technol. 139 (2004) 40– 54.

[12] S. Niedballa, Dispergierung von feinen Partikelfraktionen in Gasströmungen - Einfluss von Dispergierbeanspruchung und oberflächenmodifizierenden Zusätzen. PhD thesis, Freiberg, (1999).

[13] A. Kwade, Wet comminution in stirred media mills - research and its practical application. Powder Technol., 105 (1999) 14-20.

[14] K. Schönert, in Ullmann's Encyclopedia of Industrial Chemistry, Vol. B2, 1-5, VCH Verlagsgesellschaft, Weinheim (1988).

[15] A. Kwade, Determination of the most important grinding mechanisms in stirred media mills by calculating stress intensity and stress number. Powder Technol., 105 (1999) 382-388.

[16] M. Becker, A. Kwade, J. Schwedes, Stress intensity in stirred media mills and its effects on specific energy requirements. Int. J. Min. Proc., 61 (2001) 189-208.

[17] C. Knieke, C. Steinborn, S. Romeis, W. Peukert, S. Breitung-Faes, A. Kwade, Nanoparticle production with stirred-media mills: opportunities and limits. Chem. Eng. Technol. 33 (2010) 1401-1411.

[18] U. Prüße, J. Dalluhn, J. Breford, and K.-D. Vorlop, Herstellung sphärischer Partikel mit dem Strahlschneider-Verfahren. Chem. Ing. Tech., 72, (2000) 852–858.

[19] Y. Wu, C. Bao, and Y. Zhou, An innovated tower-fluidized bed prilling process. Chinese Journal of Chemical Engineering, 15 (2007) 424–428.

[20] T. Grassler, K.-E. Wirth, X-ray computer tomography - potential and limitation for the measurement of local solids distribution in circulating fluidized beds. , Chemical Engineering Journal, 77 (2000) 65 – 72.

[21] Y. Cheng, C. Wu, J. Zhu, F. Wei, and Y. Jin, Downer reactor: From fundamental study to industrial application. Powder Technology, 183 (2008) 364–384.

[22] W. Kaiser, Kunststoffchemie für Ingenieure. Hanser Verlag, München (2011).

[23] P. Eyerer, T. Hirth, and P. Elsner, Polymer Engineering. Berlin, Heidelberg: Springer-Verlag (2008).

[24] J. Brandrup, E. Immergut, E. Grulke, 'Polymer Handbook.4th Edition, (1998).

[25] D. Lide (Ed.), Handbook of Chemistry and Physics, 84th Edition, CRC Press , Boca Raton, FL (2003).

[26] J. Frenkel, Viscous flow of crystalline bodies under the action of surface tension. Journal of Physics, 9 (1945), 5, 385-391.

[27] N. Rosenzweig, M. Narkis, Sintering rheology of amorphous polymers. Polymer Eng. Sci., 21 (1981) 1167–1170.

[28] A. Siegmann, I. Raiter, M. Narkis, and P. Eyerer, Effect of powder particle morphology on the sintering behaviour of polymers. J. Mater Sci., 21 (1986) 1180–1186.

[29] S. Wu, Surface and interfacial tensions of polymer melts. II. Poly (methyl methacrylate), poly (n-butyl methacrylate), and polystyrene. J. Phys. Chem., 74 (1970) 632-638.

[30] M. Kirchhof, H.-J. Schmid, W. Peukert, Three-dimensional simulation of viscous-flow agglomerate sintering. Physical Rev. E, 80 (2009) 026319.

[31] S. Wu, Polymer Interface and Adhesion, 1st ed., CRC Press, New York (1982).

[32] D. W. van Krevelen and K. te Nijenhuis, Properties of Polymers: Their Correlation with Chemical Structure. Elsevier Science, Amsterdam (1990).

[33] Y. Lipatov, Structure, mechanical, and rheological properties of polyethylene–poly (oxymethylene) blends. J. Appl. Polymer Sci., 22 (1978) 1895-1910.

[34] M. Götzinger, W. Peukert, Adhesion forces distributions on rough surfaces. Langmuir 20 (2004) 5298-5303.

[35] H. Zhou, W. Götzinger, W. Peukert, The influence of particle charge and roughness on particle-substrate adhesion. Powder Technol. 135-136 (2003) 82-91.

[36] H. Rumpf, Die Wissenschaft des Agglomerierens. Chem. Ing. Tech. 46 (1974) 1–11.

[37] J. Tomas, S. Kleinschmidt, Verbesserung der Fließfähigkeit feiner kohäsiver Pulver durch nanoskalige Fließhilfsmittel. Chem. Ing. Tech. 81 (2009) 717–733.

[38] L. G. Austin, Understanding ball mill sizing. Ind. Eng. Chem. Process Des. Dev. 12 (1973) 121-129.

[39] H. Weit, J. Schwedes, Scale-Up of Power Consumption in Agitated Ball Mills. Chem. Eng. Technol. 10 (1987) 398-404.

[40] R. Pfeffer, R. N. Dave, D. Wei, M. Ramlakhan, Synthesis of engineered particulates with tailored properties using dry particle coating. Powder Technol. 117 (2001) 40-67.

[41] J. N. Israelachvili, Intermolecular and surface forces. 3rd ed., Academic Press, Waltham, MA (2011).